

Kinetics of the Physical Changes and Gas Storage Capacity Induced by Carbon Dioxide Sequestration in Coal

C. Özgen Karacan (karacan@pnge.psu.edu)
Phillip M. Halleck, Abraham S. Grader, Gareth D. Mitchell

The Pennsylvania State University-Energy Institute and Department of Energy and Geo-Environmental Engineering

Abstract

This study presents the sorbed carbon dioxide (CO₂) concentration and swelling to reveal the kinetics of the complex, heterogeneous processes occurring with CO₂ injection in a bituminous coal sample. The time-dependent swelling and gas adsorption kinetics have been quantified using dual-energy X-ray CT (X-ray computed tomography) imaging of the coal kept under in-situ stress conditions. Spatial distributions of density and effective atomic number were calculated. Coal units with changing structure, composition and geological history react differently to the injection of CO₂. Atomic number and bulk density maps enabled to decompose the amount of gas sorption and the changes in the coal matrix separately in a confined coal. Petrographic and SEM analysis of the recovered sample were used to correlate swelling and sorption behavior with local microlithotypes and microstructures.

1. Introduction

Coal-seam sequestration of CO₂ involves challenging scientific questions due to the chemically and structurally complex nature of coal. This complexity creates challenges in understanding the subsurface behavior of injected gas and coal during storage in different coal materials, which are derived from different organic materials and probably experienced diverse maturation histories. These different units usually have a wide distribution of pore sizes and have different adsorption affinities towards CO₂. Macropores within different lithotypes allow fast transport of gas into and out of the porous structures. Micropores have the function of trapping the gas within the micropore network. The micropores add additional molecular interaction between gas molecules and the coal material. Adsorption heterogeneity can also arise at this level due to distribution in size and irregular shape of the micropores (Kapoor & Yang, 1989). Within macro and micropores, the transport mechanisms acting over the macroscopic length scale of an adsorbent particle are macropore (molecular and/or Knudsen) diffusion and often also surface (sorbed phase) diffusion.

Coal type effects on gas emission are poorly understood and usually overshadowed by coal rank effects. Recent investigations of small, hand-picked samples and using high-pressure microbalances provided clear distinctions between coal type and rank with respect to gas emissions (Beamish and O'Donnell, 1992; Crosdale and Beamish, 1993; Levine et al., 1993). Gas desorption rate investigations performed by Crosdale et al. (1998) showed that bright, vitrinite-rich coals usually have the slowest

desorption rates. Some dull, inertinite-rich coals may rapidly desorb due to predominance of large, open-cell lumina.

The effect of coal composition, particularly the organic fraction, upon gas sorption capacity has been investigated for Bowen Basin and Sydney Basin coals (Laxminarayana and Crosdale, 1999). Maceral composition influences on gas retention and release were investigated using isorank pairs of hand-picked bright and dull coal in the rank range of high volatile bituminous to anthracite. It was suggested that the importance of maceral composition on maximum adsorption capacity varies according to the rank. At ranks higher than medium to low volatile bituminous, changes in maceral composition may exert relatively little influence on adsorption capacity. Dull coals desorbed more rapidly than bright coals and desorption rate was a function of the coal rank.

However, the complications arising during the injection of CO₂ into coal are not limited to the difficulties in understanding the transport and adsorption kinetics of the coal matrix. CO₂ injection into coal seams modifies the physical structure of the coal matrix. The relaxation of macromolecular structure of coal changes the pore structure. The swelling process plays an important role in determining how fast the coal can take up additional solvents. In the case of CO₂, significant swelling or volume increases ranging from 0.75 to 4.18 % were observed (Reucroft, 1987) in a range of coal samples when they were exposed to CO₂ at pressures up to 15 atm. Increase in pressure produced an increase in the swelling response and a decrease in the time required to reach maximum response. This confirms that there is a kinetic process involved in the swelling. Also, it was seen that a lower carbon content correlates with a higher degree of swelling.

For the case of organic liquid diffusion in coals, the process is similar in many respects to the diffusion of solvents in glassy polymers (Fickian diffusion or "Case II" relaxation of macromolecular structure). Therefore, swelling of coals occurs by processes that have been well documented for other macromolecular (polymer) systems (Otake and Suuberg, 1997). However, unlike other substances, it has been shown (Cody et al., 1988) that coals possess anisotropic behavior in swelling and the degree of swelling is larger perpendicular to the bedding compared to parallel to the bedding, where bond density is larger. This behavior and the anisotropic structure of coal has been attributed to the stress conditions under which the coal was generated. Mined coals are in strained state, but since the molecular motion is very slow, they can not relax from this state rapidly to reach and maintain an equilibrium state with minimum energy conformations until they are introduced with a solvent.

The changes in the initial reservoir properties of the seam, and the resultant gas transport and storage, are time- and pressure-dependent. Thus, it is necessary to define the subsurface kinetics of sorption-induced swelling and gas transport, which would represent the behavior of coal under changing gas pressures and at the presence of a confining stress. The availability of such knowledge may allow adjustment of existing coalbed methane models for the effects of swelling and gas transport changes especially during the early stages of injection.

This study presents quantitative, time-resolved spatial maps of coal density and effective atomic number and the analysis of the sorbed CO₂ concentration and swelling to reveal the kinetics of the heterogeneous processes occurring with CO₂ injection. The time-dependent swelling and gas adsorption kinetics have been quantified using dual-

energy X-ray CT (X-ray computed tomography) imaging of the coal under in-situ stress conditions. Analysis of the two independent X-ray energy data sets yield maps of density and effective atomic number distributions in the coal. Petrographic and SEM analysis of the recovered sample were used to correlate swelling and sorption behavior with local microlithotypes and microstructures.

2. Basic physics behind the dual-energy X-ray concept

X-ray CT is a non-destructive testing method based on attenuation of X-ray energies (μ) while passing through the objects. The technique was initially developed for medical applications and has been widely used for both medical and industrial applications since then. The technique consists of passing a beam of X-ray through the object from various angles and measuring the attenuation of the X-ray energy from the incident energy (Fig. 1). The attenuations measured from different angles are collected and processed by a computer to reconstruct the internal structure of the scanned object in terms of attenuation numbers.

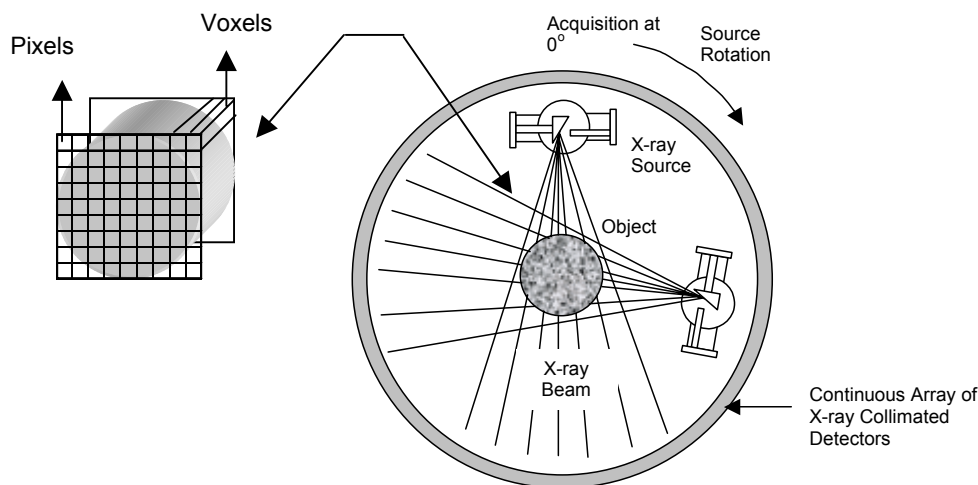


Fig. 1. The mechanics of X-ray tomography.

Conventional X-ray computed tomography systems provide cross sectional images of the investigated object by mapping the local X-ray attenuation values, which depend on the density and chemical composition, in individual image elements called pixels.

Unless density and chemical composition effects can be separated quantitatively, the images give some qualitative idea about the distribution of the materials within the object. Dual-energy X-ray scanning enables the determination of density and composition from CT data, and thus enables the quantitative investigation of the material.

The variation of the attenuation properties with different beam energies is significantly different for most materials, making possible the use two different energies at the same location in order to determine the energy-independent physical parameters, such as electron density and average atomic number. Dual-energy scanning involves use of two different beam energy spectra to distinguish the effects of different components in mixtures.

At energy levels below 200 kV, attenuation of X-rays is known to be dependent mostly photoelectric (is a function of atomic number and density of material) absorption and Compton scattering (is a function of electron density). Photoelectric absorption dominates at lower energies and becomes more important at higher atomic number. Compton scattering dominates higher energies and becomes more dominant at lower atomic number. The relation between attenuation of X-rays and density and atomic number can be represented as (Curry et al., 1990):

$$\mu = \rho \left(a + b \frac{Z^{3.8}}{E^{3.2}} \right) \quad (1)$$

In the equation ρ is bulk density, Z is bulk atomic number of the material, and E is the X-ray energy. The first term in the paranthesis is Compton scattering term and the second is photoelectric absorption term. In the equation a and b are energy dependent constants. For mixtures of atoms, an effective atomic number (Z_e) is used instead of Z . For given experimental conditions, the different interaction probabilities between photons and matter (Rayleigh, Compton, photoelectric, ...) in the case of a single element material is strongly linked to the atomic number Z . In contrast, for multiple element material, the so-called "effective atomic number" Z_e , can be used. Its aim is to completely characterize the material, in the same way that the Z value is characteristic of a single element (Duvauhelle, et al., 1999).

There are different definitions of effective atomic number in the literature. The main difference between them is the fact that some methods consider only the atomic numbers of the present elements in the mixture and their concentrations, while others also take into account the scattering angle and the photon energy. One of the most widely used methods for determining the effective atomic number below 150 kV was given by Tsai and Cho (1976):

$$Z_e = \left(\sum f_i Z_i^{3.8} \right)^{1/3.8} \quad (2)$$

Here, f_i is the fraction of the total number of electrons contributed by element i and Z_i is the atomic number of element i . In Eq. 2, f_i is treated as electronic percentage and can be defined as (Tsai and Cho, 1976):

$$f_i = \frac{(\omega_i / A_i) Z_i}{\sum_i (\omega_i / A_i) Z_i} \quad (3)$$

where ω_i is the mass percentage, and A_i is the atomic mass.

Schätzler (1978) proposed a formula where the atomic number of each element is weighted by the mass percentage, ω_i , of each element:

$$Z_e = \sum_i \omega_i Z_i \quad (4)$$

This equation is similar to the one used to calculate the mass attenuation coefficients of a compound:

$$\frac{\mu}{\rho} = \sum_i \omega_i \left[\frac{\mu}{\rho} \right]_i \quad (5)$$

however, it does not take into account the energy of photons and the scattering angle.

Scanning homogeneous calibration materials at two different energies enables determination of attenuation of X-rays (μ) in these specimens of known density and atomic number. Plotting the density and atomic number versus attenuation values of calibration materials the determination of the a and b values by using Eqs. 1 and 2 in a linear regression. Once these values are defined for two different energies (h: high, l: low), the following equations can be used to extract density and atomic number of the unknown material at each pixel position (x,y) independently (Van Geet, et al., 2000):

$$\rho(x, y) = \frac{b_h \mu_l(x, y) - b_l \mu_h(x, y)}{b_h a_l - b_l a_h} \quad (6)$$

$$Z(x, y) = 3.8 \sqrt{\frac{a_l \mu_h(x, y) - a_h \mu_l(x, y)}{b_h \mu_l(x, y) - b_l \mu_h(x, y)}} \quad (7)$$

3. Experimental section

3.1. Sample

The sample used in the CO₂ sequestration test was a high-volatile bituminous coal from Pittsburgh seam (DECS-12). The bulk sample that was preserved under argon atmosphere was cored to obtain a cylindrical sample (2.5-cm in diameter and 2-cm in length) parallel to the bedding planes. The average elemental composition of the sample was: 74.78% C, 5.11% H, 1.23% N, 1.12% S, 7.51% O. The sample had 2.5% moisture as received and left 10.25% of initial weight as ash in proximate analysis.

3.2. CO₂ sequestration test

The experimental set-up used in this investigation is shown in Fig. 2. For the visualization of CO₂ sequestration, a fourth-generation medical scanner was used. The pixel resolution and the image thickness were 0.25-mm, and 2-mm, respectively. Two energy levels used in scanning were 130-kV and 80-kV with and X-ray intensity of 65-mA.

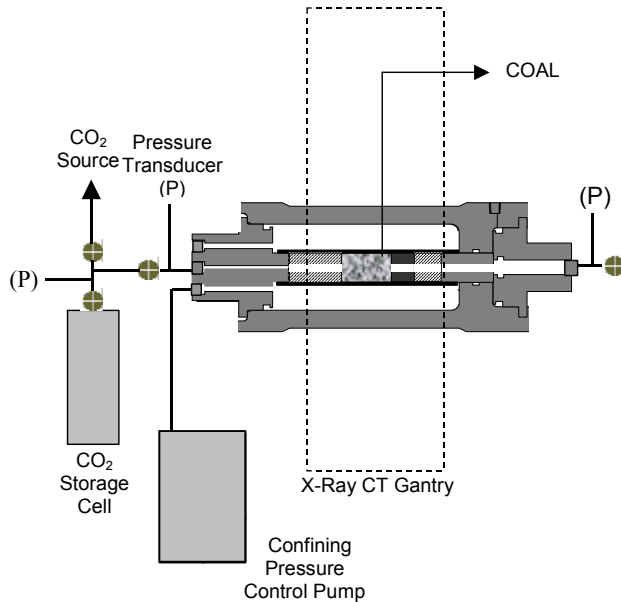


Fig. 2. Schematics of the experimental set-up.

The constant pressure gas injection has been achieved with a 1-liter capacity high-pressure gas cylinder. Pressure transducers, and a high-precision pump were used to keep track of the gas pressure and also to keep the confining pressure at a constant level. Since the pore volume of the coal sample was small in comparison to the gas-cylinder volume, this cylinder was capable of maintaining constant gas pressure on the sample at all times during the experiment.

Before starting the sequestration experiment, the confining pressure on the sample was set to 1.36-MPa. This was the effective pressure that was kept constant throughout the experiment. The sample was scanned to establish the evacuated condition of the sample. After these scans, the CO₂ that was stored in the pressure cell at 1.7-MPa was slowly released into the sample holder, while at the same time the confining pressure on the sample was increased to 3.06-MPa. Scanning of the sample, more frequently at the beginning, was continued until there was almost no or very little change in the X-ray absorption data due to further gas uptake. The last scanning sequence was taken as the adsorption equilibrium point for that pressure level and the image data represented the equilibrium stage (after 7240 minutes). After adsorption equilibrium was reached, the sample was isolated and the pressure cell was pressurized to 3.06-MPa pressure with additional CO₂. After pressure and temperature equilibrium, the gas at 3.06-MPa was applied to the sample and the confining pressure was increased to 4.42-MPa to keep the effective stress constant. Scanning was performed at this pressure level until adsorption equilibrium in the sample was attained (after another 7240 minutes). The same procedure was repeated when the gas pressure was increased to 4.42-MPa and confining pressure was increased to 5.78-MPa. The equilibrium at this stage was reached after 5000 minutes. The experimental pressure-time sequence is shown graphically in Fig. 3. This experimental methodology enables the experiment to be conducted at three different gas pressures to follow the kinetics of gas storage and matrix property changes at three different gas pressures while keeping the sample under constant effective stress.

3.3. Use of phantom materials for dual-energy calculation

The use of dual-energy X-ray scanning to determine physical parameters such as density and atomic number requires determination of X-ray attenuation properties of materials of known density and atomic composition as explained in Section 2. For this

purpose, water, benzyl alcohol and fused quartz phantoms were scanned in the core vessel to determine the attenuation properties at 130 and 80-kV and 65 mA.

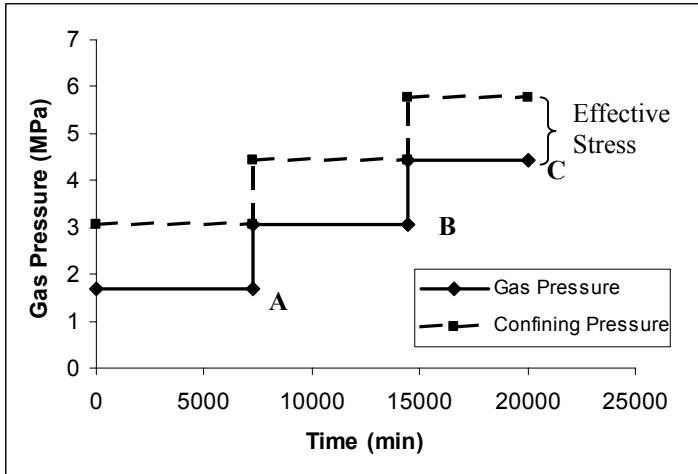


Fig. 3. Pressure-time history of the test (A: 1.7, B: 3.06 and C: 4.42-MPa)

These substances were selected to cover the possible range of density and atomic number of carbon dioxide and coal. Table 1 gives the X-ray attenuations (in Hounsfield units), densities and effective atomic numbers of these substances that were used to determine constants a and b of Eq. 1.

Table 1. X-ray attenuations (as CT numbers), densities and effective atomic numbers of these substances that were used to determine constants a and b of Eq. 1.

	ρ (g/cc)	Z_e	CT number 130 kV	CT number 80 kV
Benzyl alcohol	1.04	5.92	65.9	260.1
Water	1.00	7.54	82.4	322.0
Fused quartz	2.65	11.81	930.9	1455.9

The CT numbers given in Table 1 were used to correlate density and effective atomic numbers of the known substances to generate a general equation, for the particular scanning conditions, with constants a and b to extract the local bulk density and effective atomic number of the coal sample with and without CO₂.

4. Results and discussion

Sorption and gas transport kinetics are essential for predictive calculations and reservoir modeling efforts of CO₂ sequestration in coal seams. Evaluation and quantification of these properties on consolidated cores kept under a constant effective stress has been performed before (Karacan and Okandan, 2001, Karacan and Mitchell, 2003, Karacan, 2003) to investigate the sorption kinetics and behavior of different microlithotypes under CO₂ pressure. In these studies X-ray CT was used with a single-energy approach. With proper calibration and image quantification, application of a high energy X-ray beam resulted in maps, which were *mostly* functions of density variations in the sample due to CO₂ injection. In these studies, the most general conclusions were the superiority of the imaging technique to extract spatial distribution of sorption kinetics data in different microlithotypes, and the high storage capacity associated with clay+inertite layers and the fast diffusion rates associated with higher porosity. In these

studies, it was concluded that in some of the microlithotypes (e.g liptite), surface diffusion increases with increasing pressure. Also, after calculations for the increase in density due to CO₂ loading, an effective density decrease has been observed, especially for vitrite layers, due to coal swelling. The change in density in those layers could not be directly attributed to the net amount of swelling, because it was not possible to decompose the amount of gas stored from the matrix effects with a single energy level.

In this study, dual-energy scanning enabled the direct characterization of the studied materials in terms of density and chemical composition. Figure 4 gives the resolved bulk density and atomic number map of the coal after about 20000 minutes of CO₂ injection at 4.42 MPa gas pressure and after normalizing by the initial properties of the coal.

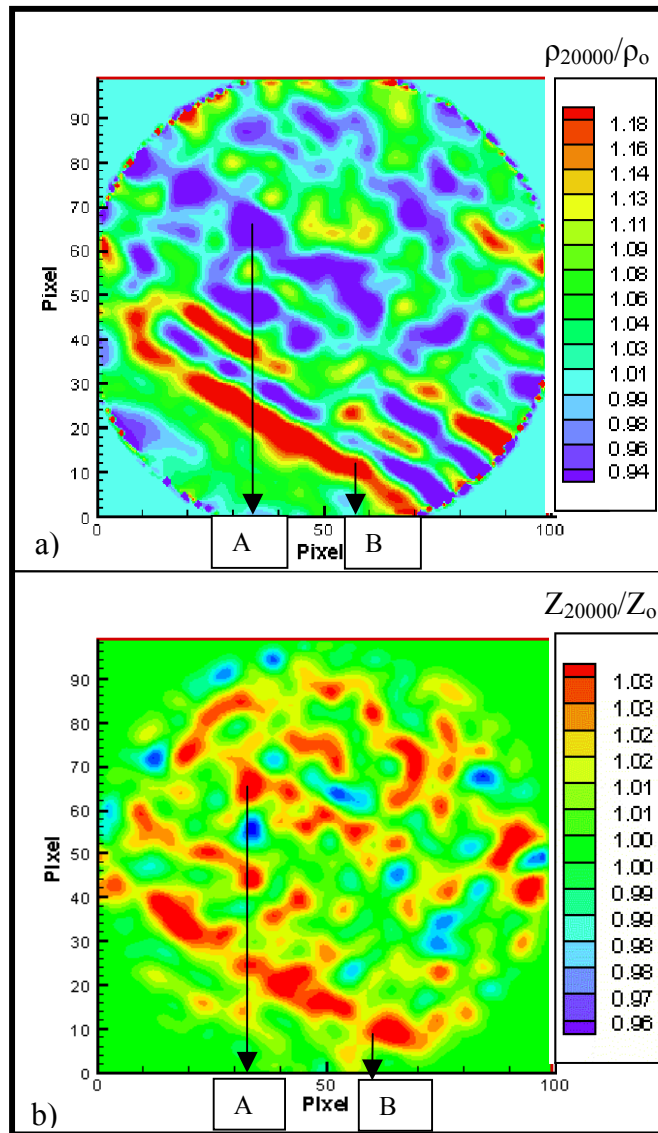


Fig. 4. Normalized bulk density (a) and effective atomic number (b) maps of the coal (after dividing the 20000 minutes data by the 0 minute data).

The density map in Fig. 4 shows that in some of the regions, the density of the coal matrix has increased (B) and in some regions it has decreased (A) compared to the initial density. This can only be possible if the volume of the coal is changing in region A. Comparison of density map with the effective atomic map at the same locations shows that in both regions the effective atomic number has increased, suggesting storage of higher amount of CO₂ in both regions. But, the behavior of B is different than A, possibly due to the differences in microlithotype. The microlithotype analyses by optical microscope and SEM analysis (Fig. 5) in these two regions show that A is mostly microporous vitrite type microlithotype, and B is a mixture of clay+quartz+inertite. Vitrite is known to swell when exposed to CO₂ gas. Energy dispersive scan (EDS) analysis performed showed that in both places, the mineral phase is rich in Si and Al, suggesting that the minerals are clay type minerals. There is higher amount of Si due to quartz in region B.

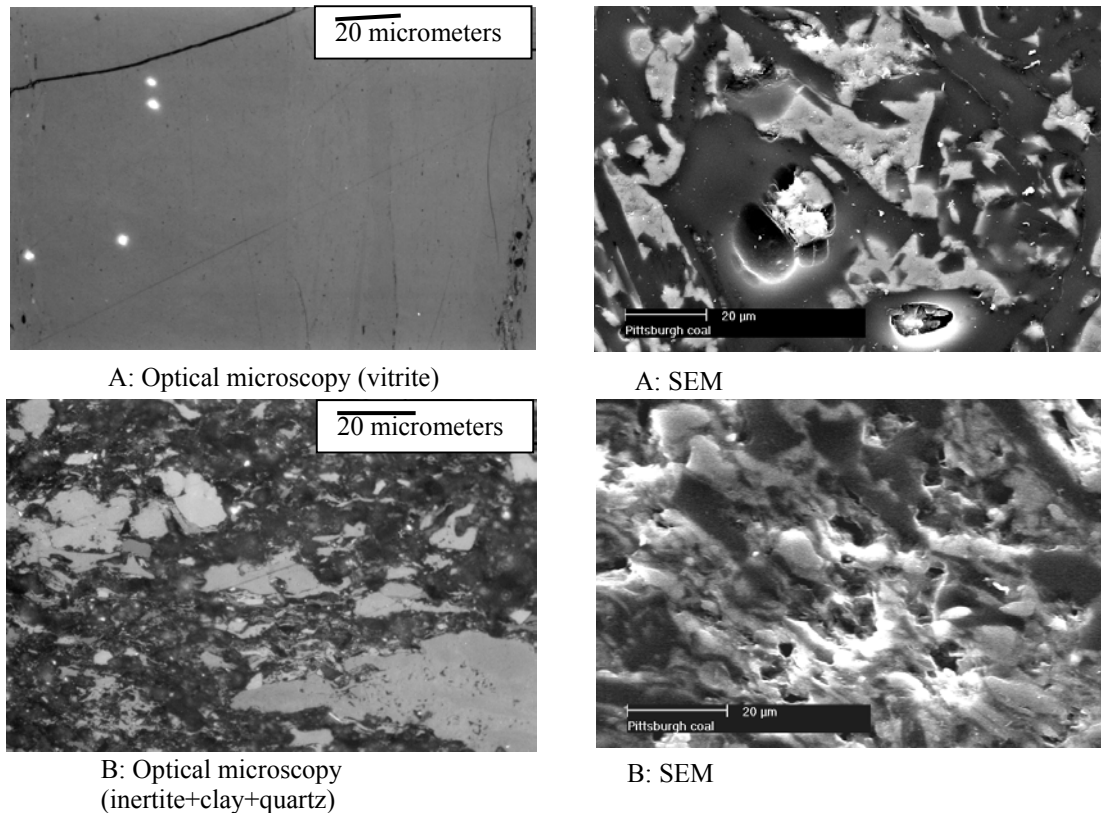


Fig. 5. Optical microscopy and SEM images from regions A and B shown in Fig. 4

Figures 4 and 5 demonstrate that various coal microlithotypes respond differently when they are exposed to CO₂ injection. The response of coal to CO₂ injection depends on the chemical structure of the organic materials that goes through different rearrangements, and the interaction and solution of CO₂ in various macerals.

Figure 6 shows the kinetics of the density change at specific locations within the sample.

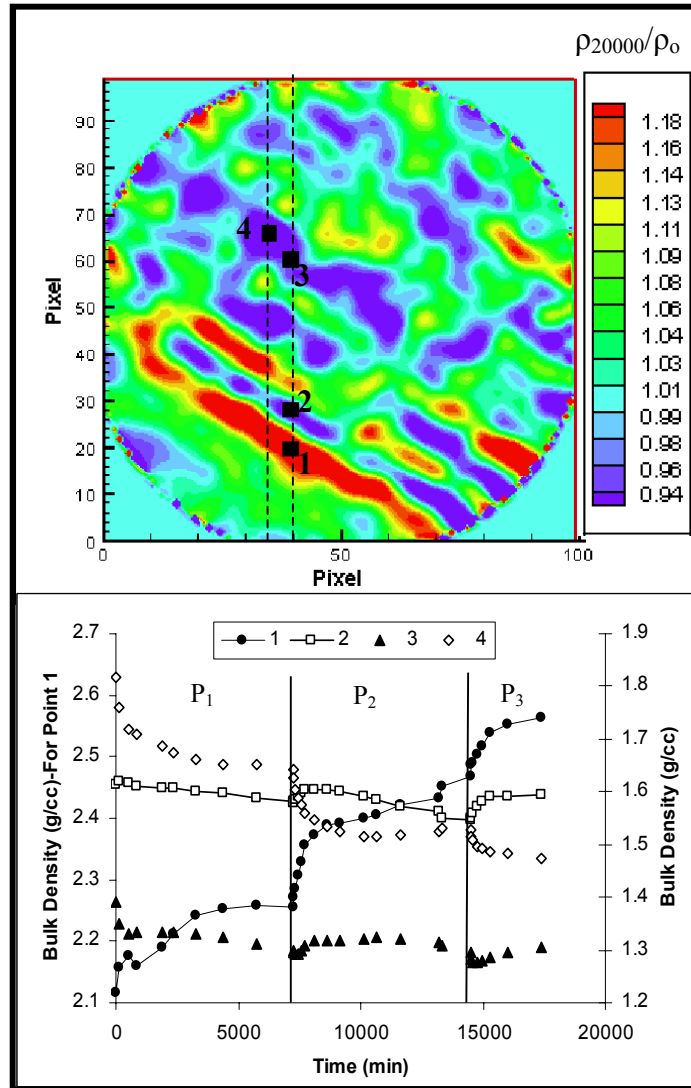


Fig. 6. Kinetics of bulk density changes at selected points (P_1 : 1.7, P_2 : 3.06 P_3 : 4.42-MPa).

In Fig. 6, the regions 2, 3, and 4 follow kinetics different than point 1. The bulk density of point 1 increases with time as the pressure is increased. This shows that the swelling effect is not present or not pronounced at this point. However, at points 2, 3, and 4, the bulk density decreases in general with time with increasing gas pressures, indicating swelling. At these points, what is interesting is that the bulk density shows an increasing trend also especially when the gas pressure first increased. This “*breathing*” behavior is due to adsorption and diffusion of gas molecules into the macromolecular structure of the coal, followed by a subsequent swelling. The behavior of the coal matrix and the different kinetics of gas storage and swelling suggest that the rate of density change can be different at each different pressure step.

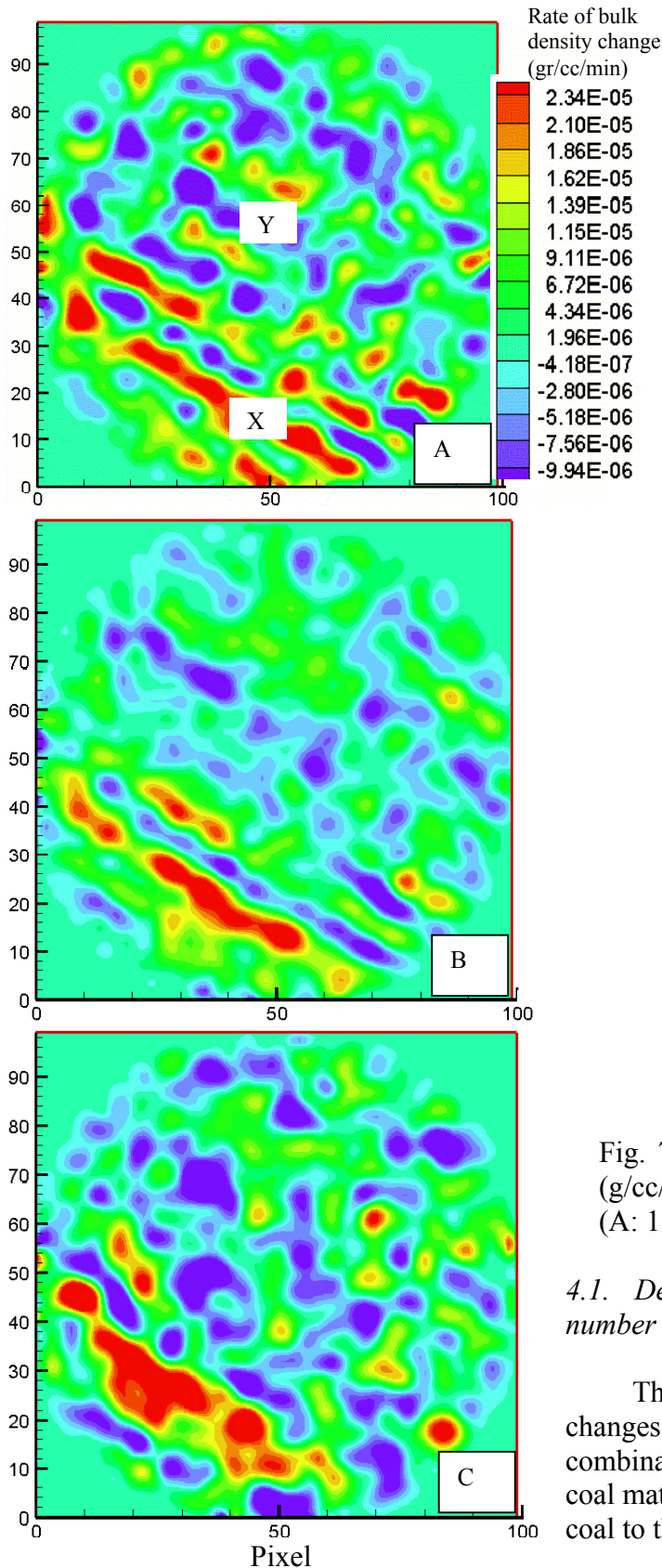


Figure 7 shows the rate of density change map in the coal as calculated by dividing the differential amount of density at each pressure by the total duration that the gas was applied at that pressure step (Fig. 3). This figure clearly shows that, the inertite+clay (X) layer takes gas to increase the density at a high rate at 1.7 MPa pressure. The density of vitrite layers (Y) decreases with a high rate again due to gas diffusion and matrix relaxation. At a pressure of 3.06 MPa, the density of the inertite layer continues to increase. However, at regions along that layer, rate of density increase decreases. In the vitrite layer, which is in the middle of the sample, the swelling rate decreases. When 4.42-MPa CO₂ gas pressure was applied, the rates of bulk density changes increase again. The kinetics plot given in Fig. 6 and the rates of bulk density changes given in Fig. 7 shows that the gas storage and matrix swelling kinetics are not linear functions, or proportional to the gas pressure applied. The kinetics of these processes is complex functions of diffusion, adsorption, absorption and the swelling of the macromolecular network of coal with time and gas pressure applied.

Fig. 7. Average rate of bulk density change (g/cc/min) at different gas pressure regimes (A: 1.7, B: 3.06 and C: 4.42-MPa).

4.1. Decomposition of density and atomic number maps into gas and coal matrix maps

The density and effective atomic number changes and the maps given up to this point are combinations of the accumulation of gas in the coal matrix (gas amount) and the response of the coal to this effect (swelling).

However, as mentioned before, dual-energy scans can be used to decompose the amount of gas and the changes in the matrix. For this purpose, CO₂ and local coal matrix were considered as simple elements with Z_{eff} electrons per atom (Duvauchelle et al., 1999). This allowed establishing an analogy with the classical atomic model and the use of Eq. 4 to calculate the mass percentages of CO₂ and coal matrix at any given time during pressurizing the coal by using total effective atomic number distribution. Then, bulk mass maps were created by multiplying bulk density map with the volume of voxels (0.00125 cc). The mass fractions of CO₂ and coal calculated from effective atomic number maps have been used to calculate the mass amount of gas and coal matrix separately from bulk mass maps.

Figure 8 presents the maps of net gas accumulated (as $g.CO_{2@t}/g. \text{ of initial coal mass}$) and the net change of coal matrix mass ($m_{\text{coal}@t}-m_{\text{coal}@i}/m_{\text{coal}@i}$). The calculations presented as maps were performed at the equilibrium stages (A, B, and C in Fig. 3) of each pressure step. The net mass change maps given in Fig. 8 show that gas storage increases at each pressure step. The gas storage is larger in inertite+clay and vitrite layers and the amount increases with increasing gas pressure. The maximum amount of gas stored is about 0.138 g/g in inertite+clay layer. In vitrite layer, the amount of gas stored is between 0.06-0.08 g/g. Comparing gas storage maps with the coal matrix mass change maps shows that the changes occurring in the matrix well coincides with the gas-stored regions especially in vitrite layers. The maximum amount of mass difference in the particular voxels (due to swelling) is about 0.1 g/g of initial mass. In the other regions, no negative mass change was calculated. In fact, there was some amount of mass increase in the coal matrix. This may be due to the possible chemical changes in the coal matrix compared to the initial state or squeezing of the matrix (since the total volume was kept more or less constant with the confining pressure) due swelling in the vitrite bands.

5. Conclusions

CO₂ storage into coal has shown that the swelling and gas sorption in coal are heterogeneous processes. Vitrite microlithotype has shown a major amount of swelling effect as determined from bulk density variations in those regions. The overall density decreases by upto 0.3 g/cc in some regions due to swelling. On the other hand, the bulk density in inertite+clay regions increases by about 0.4 g/cc due to additional carbon dioxide accumulation. The kinetics behavior of these processes show that in vitrite and mostly organic regions, density increases when the gas pressure was increased and then starts to decrease again, “breathing”, suggesting the presence of a solution process and relaxation of coal matrix.

The rates of bulk density change with time in each pressure regime are different also. It was calculated and mapped in the coal that the rates of density changes due to gas storage and swelling are not proportional to the gas pressure applied.

The decomposition of atomic number maps to net coal mass and net gas storage enabled to calculate the change of matrix properties and gas storage amount. The data indicates that the highest amount of gas is stored in inertite+clay regions (~0.1 g/g.coal), followed by vitrite layers (~0.08 g/g). However, the behavior of their matrix properties was quite different. Vitrite was calculated to swell to decrease the initial mass of the matrix by more than 0.1 g.coal/g.coal. At the same time, the mass change of clay+inertite

region is about 0.07-0.16 g/g. to increase the mass. This may be due to compression of clay layers as a response to expansion in vitrites in a confined system.

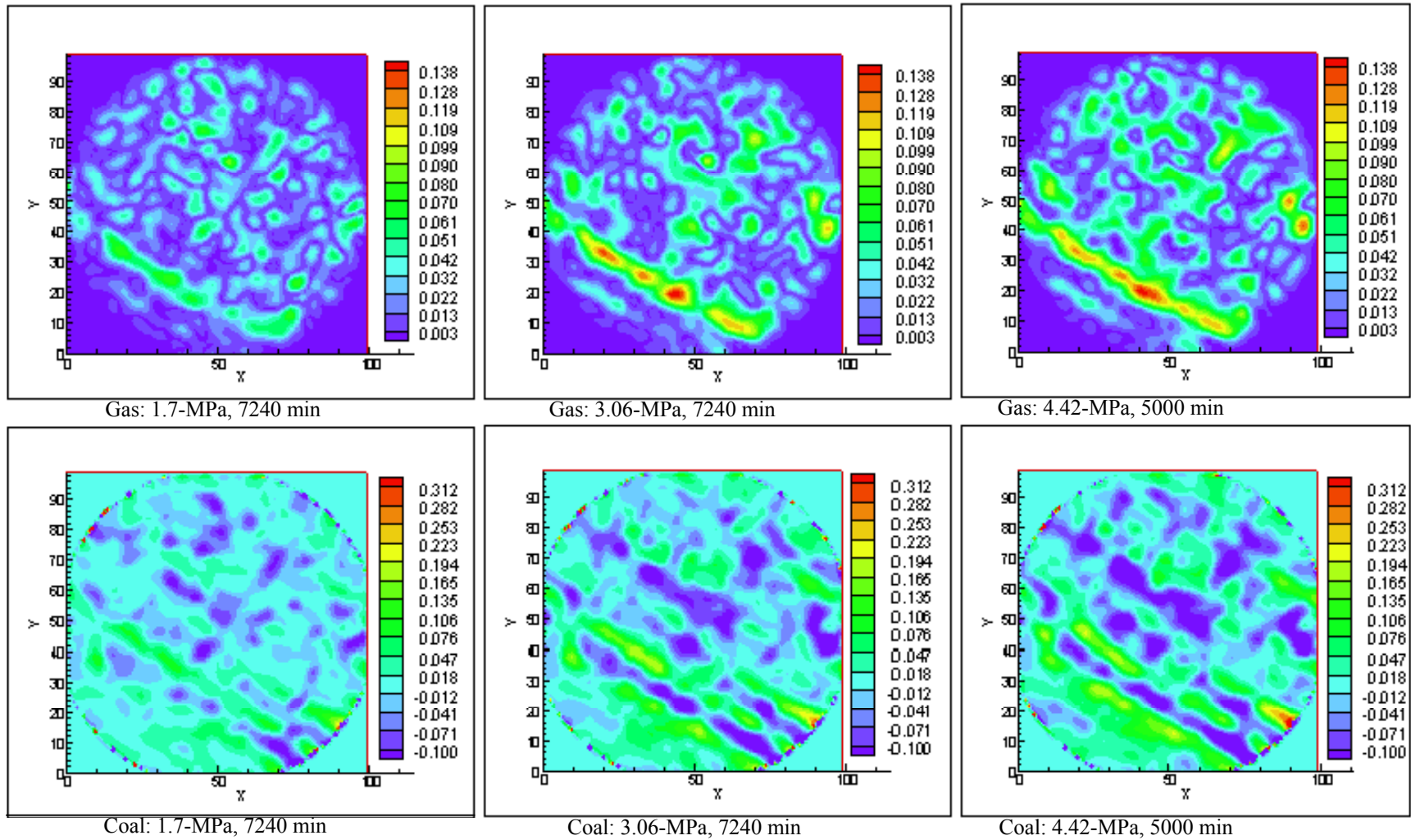


Fig. 8. The maps of net gas amount stored in coal (top row) and the change in the coal matrix (bottom row) at the end of each pressure step. Legend in the top row is in $\text{g. CO}_2/\text{g.coal}$, and the legend in the bottom row is $\Delta\text{g.coal}/\text{g.coal}_{(\text{initial})}$.

References

- Beamish, B.B., and O'Donnell, G., 1992. Microbalance applications to sorption testing of coal. Symp. Coalbed Methane Research and Development. Vol. 4. Dept. Earth Sci., James Cook Univ., Townsville, 31-41.
- Cody, G.D. Jr, Larsen, J.W., Siskin M., 1988. Anisotropic solvent swelling of coal, *Energy and Fuels*, 2, 340-344.
- Crosdale, P.J., and Beamish, B.B., 1993. Maceral effects on methane sorption by coal. In: Beeston, J.W. (Ed.) *New Developments in Coal Geology: A Symposium*. Coal Geol. Group, Geol. Soc. of Australia. Brisbane, 95-98.
- Crosdale, P.J., and Beamish, B.B., and Valix M., 1998. Coalbed methane sorption related to coal composition. *Int. J. Coal Geol.* 35, 147-158.
- Curry, T.S., Dowdey, J.E., and Murry, R.C.Jr., 1990. Christensen's physics of diagnostic radiology. 4th Edn. Lea and Febiger, Philadelphia.
- Duvauchelle, P., Peix, G., and Babot, D., 1999. Effective atomic number in the Rayleigh to Compton scattering ratio. *Nuclear Inst. And Meth. In Phys. Res. B.* 155, 221-228.
- Geet, M.V., Swennen R., and Wevers M, 2001. Quantitative analysis of reservoir rocks by microfocus X-ray computerized tomography. *Sedim. Geol.* 132, 25-36.
- Kapoor, A. and Yang, R.T., 1989. Surface diffusion on energetically heterogeneous surfaces. *AIChE Journal.* 35, 1735-1738.
- Karacan, C.Ö., and Okandan E., 2001. Adsorption and gas transport in coal microstructure: investigation and evaluation by quantitative X-Ray CT imaging. *Fuel.* 80, 509-520.
- Karacan, C. Ö., and Mitchell G.D., 2003. Behavior and effect of different coal microlithotypes during gas transport for carbon dioxide sequestration into coal seams. *Int. J. of Coal Geol.* 4, 201-217.
- Karacan C. Ö., 2003. An effective method for resolving spatial distribution of adsorption kinetics in heterogeneous porous media: application for carbon dioxide sequestration in coal. submitted to *Chem. Eng. Science*.
- Laxminarayana C., and Crosdale P.J., 1999. Role of coal type and rank on methane sorption characteristics of Bowen Basin; Australia coals. *Int. J. Coal Geol.* 40, 309-325.
- Levine, J.R., Johnson, P.W., and Beamish B.B., 1993. High pressure microgravimetry provides a viable alternative to volumetric method in gas sorption studies on coal. *Proc. 1993 Int. Coalbed Methane Symp. Univ. of Alabama, Tuscaloosa*, 187-195.

Otake, Y. and Suuberg, E., 1997. Temperature dependence of solvent swelling and diffusion processes in coal. *Energy and Fuels*, 11, 1155-1164.

Reucroft, P.J. and Sethuraman, A.R., 1987. Effect of pressure on carbon dioxide induced coal swelling. *Energy and Fuels*, 1, 72-75.

Schatzler, H.P., 1978. *Int. J. of App. Radiat. Isot.* 30, 115.

Tsai, C.M., and Cho, Z.H., 1976. *Phys. Med. Biol.* 21, 544.

Unsworth, J.F., Fowler, C.S., Jones, L.F., 1989. Moisture in coal. 2. Maceral effects on pore structure. *Fuel*. 68, 18-26.